



Spin-optical solitons in liquid crystalsGaetano Assanto ¹ and Noel F. Smyth ^{2,3}¹*NooEL—Nonlinear Optics and OptoElectronics Lab, University of Rome “Roma Tre”, 00146 Rome, Italy*²*School of Mathematics and Maxwell Institute for Mathematical Sciences, University of Edinburgh, Edinburgh EH9 3FD, Scotland, United Kingdom*³*School of Mathematics and Applied Statistics, University of Wollongong Wollongong, New South Wales 2522, Australia*

(Received 4 June 2020; accepted 11 August 2020; published 1 September 2020)

In the framework of nonlinear spin optics, we investigate self-confined light beams in reorientational nematic liquid crystals. Using modulation theory and numerical experiments, we analyze spatial solitary waves supported by the geometric phase arising in a uniaxial when subject to a nonlinear modulation of its optic axis distribution. Spin evolution and optical reorientation in an index-homogeneous medium give rise to a longitudinally periodic, transversely inhomogeneous potential able to counteract the diffraction of a polarized bell-shaped beam, generating a spin-optical solitary wave. Spin-optical solitary waves evolve in polarization and have an oscillatory character in amplitude, size, and ellipticity.

DOI: [10.1103/PhysRevA.102.033501](https://doi.org/10.1103/PhysRevA.102.033501)**I. INTRODUCTION AND MOTIVATIONS**

Self-focusing of light beams via the nonlinear response of dielectrics to intense excitations is known to yield transverse confinement and diffractionless propagation into spatial solitary waves—loosely, solitons—since the early work of Chiao *et al.* [1]. In the applied mathematics literature there is a distinction between the terms solitary wave and soliton [2], but here we will use interchangeably terms such as solitary waves, solitons, self-localized beams, diffractionless wave packets, self-trapped or self-confined beams, and their combinations as this is common in the physics literature. Self-trapped wave packets have been reported in a wide variety of materials and on the basis of diverse nonlinearities, among them the quadratic cascading of parametric interactions [3] and the cubic, Kerr-like response of intensity dependent dielectrics [4]. The latter include the local response of, e.g., glass, the weakly nonlocal response of photorefractives, and the highly nonlocal response of thermo-optics, as well as of nematic liquid crystals [5–7]. Nonlocality, i.e., the material's ability to respond even at finite distances from the electromagnetic disturbance, is one of the features which allows the stability of spatial solitons in two transverse dimensions (2D), that is, in bulk [8–10]. An important benefit of 2D solitary waves in nonlocal Kerr-like media—at variance with those in quadratic crystals—is that they are normal modes of the corresponding self-induced graded-index waveguides; otherwise stated, not only do they self-trap, but they can also confine optical signals of different frequencies as long as their wavelengths can be guided by the nonlinearly sustained refractive index potential [11].

Of particular interest is the electromechanical nonlinear optical response of birefringent molecular crystals in the fluid state, referred to as the reorientational nonlinearity. The latter is common, e.g., in uniaxials such as nematic liquid

crystals (NLC), consisting of angularly aligned, nonpolar, and anisotropic molecules which, bound to one another by elastic forces, in the presence of large electric fields (at light frequencies) are able to rotate in space and yield beam self-focusing due to the resultant refractive index increase [12]. In physical terms, when a suitably polarized intense light beam propagates through the material, the torque due to the reaction of the optically induced dipoles to the electric field vector is able to change the molecular angular orientation, lowering the system energy and the phase speed of extraordinary waves [13]. The nonlinear redistribution of the refractive index, higher wherever the beam is more intense, as well as nonlocal because of the intermolecular links in the fluid, can give rise to a graded potential with light guiding properties, i.e., a waveguide preventing beam diffraction and supporting stable spatial solitons. Such (linearly polarized) solitary waves in NLC have been termed nematicons and their properties, as well as their applications, have been investigated both experimentally and theoretically in the past two decades [14–18]. We recall here that nematicons can be generated by continuous-wave beams at milliWatt powers [14], have governing equations which admit no (known) exact solutions [18,19], exhibit optical bistability versus power excitation [20,21], can be exploited in synergy with other nonlinear effects [22–25], including random lasing [26,27], and can be redirected by external voltages [28,29], beams [30,31], and magnetic fields [32–34].

Nematicons are extraordinarily (e-) polarized wave packets in uniaxial NLC, whereby the beams maintain their electric field oscillating in the principal plane of the optic axis and the wave vector. Whenever the input beam polarization (i.e., each of its plane wave components) does not match either of the two eigenwaves of the uniaxial, it excites ordinary and extraordinary waves detuned in phase velocities, so that the wave packet evolves in its “spin” state during propagation. In the presence of a nonuniformity, such as a transversely

varying orientation of the optic axis (or symmetry axis), the evolution can involve the periodic coupling of ordinary and extraordinary waves and so result in a “cascaded” process. The additional phase term generated during this polarization transformation (i.e., the path followed along the surface of a Poincaré sphere) is often referred to as the Pancharatnam-Berry (PB) geometric phase [35,36], which is linked to various phenomena in the frame of so-called “spin-orbit interactions of light” or “spin optics” [37–41]. Early work on the geometric Berry phase dealt with the propagation of linearly polarized light in the presence of homogeneous refraction [42]. Most recent optical manifestations have been associated with dielectric anisotropy in 2D metasurfaces and birefringent crystals [41,43–45], entailing several applications in photonics [46]. When the spin transformation is a pointwise function of the anisotropic distribution across the beam profile, the PB phase can alter the phase front of a propagating wave packet and yield transverse confinement, leading to novel waveguiding approaches which do not rely on total internal reflection [47–49]. Furthermore, in bulk anisotropic dielectrics, such as homogeneously aligned nematic liquid crystals, the modulation of the optic axis distribution can be nonlinearly induced through all-optical reorientation, as mentioned above. In configurations for which the optic axis is perpendicular to the beam wave vector and the input wave packet couples to both ordinary and extraordinary components (as it is not just one eigenwave), the propagation is not affected by changes in refractive index and the PB phase can be nonlinearly tailored by reorientation according to the light polarization and intensity at each point, i.e., the “local” spin. Otherwise stated, the (inhomogeneous) optic axis modulation required to provide transverse confinement via geometric phase, as described, e.g., in Ref. [47], can be obtained by the nonlinear action of a suitably polarized and shaped beam. In this limit, the input excitation can generate a reorientational spatial solitary wave with varying polarization—a “spin-optical” soliton. A pioneering experiment on such spin-orbit interaction of light was experimentally carried out in a one-dimensional setting by Karpierz *et al.*, who observed beam self-localization of mixed TE and TM beams in homogeneous (homeotropically aligned) NLC planar waveguides [50]. This early demonstration of one-dimensional spin-optical solitons was not interpreted in terms of self-confined waves and Pancharatnam-Berry phase, although the inherent roles of polarization transformation and reorientation were invoked a few years later to derive the approximate profile of such solitary waves [51]. Experimental evidence of 2D spin-optical solitons due to the interplay of PB phase and nonlinear reorientation in initially uniform samples was subsequently reported by Kwasny *et al.* in (planarly aligned) bulk NLC [52].

In this paper we afford the ambitious goal of using modulation theory [2] to model two-dimensional optical solitary waves stemming from the interplay of nonlinear reorientation and spin transformation in nematic liquid crystals. These solitary waves are not associated with a refractive index change as they stem from spin-orbit interactions, an entirely innovative approach to light guidance [47]. Such an unusual self-trapping mechanism could hold promise towards new all-optical switching schemes, as well as signal waveguiding in novel soliton-defined permanent structures in

polymerizable media [53]. These spin-optical solitons have an oscillatory character versus propagation and therefore shed radiation which cannot be totally trapped by the light-induced waveguide, as is the case for nonlocal, linearly polarized nematicons [18]. Finally, spin-optical solitons evolve to have elliptical profiles, as expected due to the inherent anisotropies in nonlinearity and diffraction.

II. MATERIAL, NONLINEARITY, AND INTERACTION GEOMETRY

Hereby, we consider nematic liquid crystals, a birefringent material with a single symmetry axis, which consists of anisotropic molecules bound in a fluid state. NLC are thermotropic liquid crystals exhibiting large birefringence, extended spectral transparency, and a reorientational response to electromagnetic fields [54,55]. Standard NLC are positive uniaxials with optic axis coincident with the molecular director \mathbf{n} , a unit vector locally aligned with the long axis of the ellipsoid-shaped molecules. For a given wave vector \mathbf{k} , the two ordinary (o-) and extraordinary (e-) plane wave eigensolutions propagate with phase velocities c/n_{\perp} and c/n_e , respectively, with c the speed of light in vacuum, $n_e(\theta) = (\cos^2 \theta/n_{\perp}^2 + \sin^2 \theta/n_{\parallel}^2)^{-1/2}$ the extraordinary refractive index, θ the angular orientation of \mathbf{n} with respect to \mathbf{k} , n_{\perp} the ordinary refractive index, and $n_{\parallel} = n_e(\pi/2)$ the upper limit of the extraordinary index. In the presence of an electric field of vector \mathbf{E} , below the so-called Freédericks threshold the optical torque acting on the induced dipoles can be cast in the form [55]

$$\mathbf{\Gamma} = \epsilon_0 \epsilon_a (\mathbf{n} \cdot \mathbf{E}) (\mathbf{n} \times \mathbf{E}), \quad (1)$$

with ϵ_0 the vacuum dielectric constant and ϵ_a the dielectric anisotropy $\epsilon_a = n_{\parallel}^2 - n_{\perp}^2$. When the initial \mathbf{E} , \mathbf{k} , and \mathbf{n} are not mutually orthogonal, an intense e-wave field can generate a torque $\mathbf{\Gamma}$ counteracting the elastic forces (intermolecular links) in the liquid and so increase θ and n_e to yield a saturable self-focusing response. This nonlinear response is therefore nonlocal and polarization preserving, and supports the propagation of nematicons [14–16]. The torque given by Eq. (1) can also act on \mathbf{n} when $\mathbf{k} \cdot \mathbf{n} = 0$, i.e., when the beam propagates orthogonally to the optic axis. In this case, a transverse electric field can reorient \mathbf{n} in the (x, y) plane according to the beam shape, altering the system anisotropy and introducing pointwise coupling between the spatially dispersive o-wave and e-wave components.

For the sake of simplicity, and with reference to the experimental evidence reported earlier, the interaction we investigate hereby for spin-optical spatial solitary waves due to a reorientation tuned geometric phase resembles the NLC configuration in Ref. [52], as sketched in Fig. 1. A coherent bell-shaped input beam with main wave vector along $\mathbf{k} \parallel z$ and electric field components E_x and E_y along x and y , respectively, propagates into planar homogeneous NLC with optic axis \mathbf{n} aligned along y . In this setting (i.e., at normal incidence with respect to \mathbf{n}), the relative dielectric susceptibility can be expressed as

$$\epsilon_{jk} = n_{\perp}^2 \delta_{jk} + \epsilon_a n_j n_k, \quad j, k = x, y, z, \quad (2)$$

with δ_{jk} the Kronecker delta and n_j the components of $\mathbf{n} = (\sin \xi, \cos \xi, 0)$. The angle ξ fully describes the optic axis

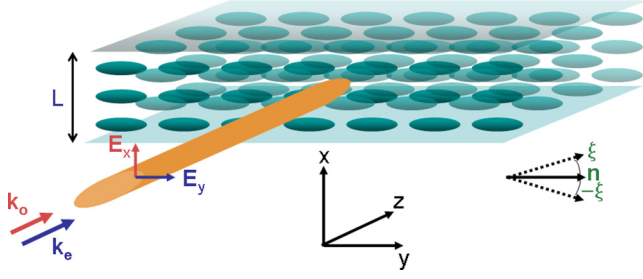


FIG. 1. Sketch of the considered sample and interaction geometry. A planar cell of thickness L contains the homogeneously aligned nematic liquid crystal. The ellipses represent the elongated NLC molecules, with long axes along \mathbf{n} and parallel to y at rest. The input light beam impinges on the sample normally to \mathbf{n} , carrying both ordinary (wave vector \mathbf{k}_o) and extraordinary (wave vector \mathbf{k}_e) components of the electric field \mathbf{E} . In the absence of longitudinal field components, the optic axis \mathbf{n} can reorient within (x, y) at an angle ξ with respect to y .

reorientation in the plane (x, y) under the action of an electric field purely transverse ($E_z = 0$) with respect to $\mathbf{k} \parallel z$. The eigenwave vectors take the values $k_o = k_0 n_\perp$ and $k_e = k_0 n_\parallel$ for electric fields oscillating along x and y , respectively. Hence an input beam encompassing both transverse components populates the o- and e-eigensolutions with a (momentum) mismatch $\Delta k = k_0(n_\perp - n_\parallel)$. In the linear regime, these eigenwaves acquire an additional phase term $\Delta\phi = \Delta k z$ when propagating along z , yielding a polarization state transformation from, e.g., linear to elliptical, circular, elliptical to linear, etc., with a beat length $l_b = 2\pi/\Delta k$ [56]. When reorientation of the symmetry axis occurs in the transverse plane (x, y) owing to the electric field distribution across the beam profile, the point dependent coupling between eigenwaves translates to a geometric phase as the latter depends on the spin evolution across the wave packet, i.e., it is nontransitive [49]. The PB phase needs to be larger on beam axis (than in its outskirts) while monotonically accumulating retardation along z in order to balance out diffraction [47]. Both these requirements are satisfied by the reorientational response, inasmuch as the nonlinearity is maximum at the beam intensity peak and exhibits a recurrent change in sign with period $\Lambda = l_b$ owing to the polarization rotation. This change in sign counteracts the sign change in PB phase accumulation due to spin evolution, so that the PB distribution in (x, y, z) resembles a “quasi-phase-matched” [57,58] three-dimensional photonic potential able to compensate spatial spreading and so guide light [47].

In the configuration described above, invoking the paraxial approximation for wave-packet propagation in a nonlocal uniaxial environment, the dimensional model for the evolution of a beam with both transverse components of the electric field and in the presence of nonlinear reorientation can be written as

$$2ik_0 n_\perp \frac{\partial E_x}{\partial z} + \frac{\partial^2 E_x}{\partial x^2} + \frac{\partial^2 E_x}{\partial y^2} + k_0^2 \epsilon_a E_x \sin^2 \xi + \frac{1}{2} k_0^2 \epsilon_a E_y e^{ik_0(n_\parallel - n_\perp)z} \sin 2\xi = 0, \quad (3)$$

$$2ik_0 n_\parallel \frac{\partial E_y}{\partial z} + \frac{\partial^2 E_y}{\partial x^2} + \frac{n_\parallel^2}{n_\perp^2} \frac{\partial^2 E_y}{\partial y^2} - k_0^2 \epsilon_a E_y \sin^2 \xi + \frac{1}{2} k_0^2 \epsilon_a E_x e^{-ik_0(n_\parallel - n_\perp)z} \sin 2\xi = 0, \quad (4)$$

with the nonlinear, nonlocal response given by

$$K \nabla^2 \xi + \frac{1}{4} \epsilon_0 \epsilon_a [2(|E_x|^2 - |E_y|^2) \sin 2\xi + 2 \operatorname{Re} E_x E_y^* e^{-ik_0(n_\parallel - n_\perp)z} \cos 2\xi] = 0. \quad (5)$$

Here, the Laplacian $\nabla^2 \xi$ is in the transverse plane (x, y) and K is the scalar strength for the elastic NLC molecule interaction in the liquid, assuming equal elastic constants for bend, splay, and twist deformations [55]. For the computational analysis we will use the material parameters of the standard E7 mixture at room temperature, a positive uniaxial NLC with $n_\parallel = 1.73$ and $n_\perp = 1.53$, and elastic constant $K = 12 pN$. Coherent and polarized Gaussian beams are launched with plane wave front at wavelength $\lambda = 1.064 \mu\text{m}$ with waist w of $2.5 \mu\text{m}$ at the origin $x = y = z = 0$ of a planar cell of size $L = 42 \mu\text{m}$ across x . The latter thickness, slightly smaller than in reported experiments [52] for which beam alignment is a crucial issue, was selected to reduce computation times, while having minimal effects on the results. It should be noted that, as long as the beams are well removed from the boundaries, the solutions for E_x , E_y , and ξ have negligible dependence on the cell size.

III. MODULATION THEORY

The paraxial Eqs. (3)–(5) used in the present work can be derived from a more general, Helmholtz-type system as in [52], and are also related to the model in [51]. The derivation of the paraxial equations involves a number of approximations and transformations which are relevant for the interpretation of the results, as will be detailed. The full, Helmholtz-type model governing the field components E_x and E_y and the director angle ξ are [52]

$$\begin{aligned} & \epsilon_a \cos^2 \xi \frac{\partial^2 E_y}{\partial x \partial y} + \frac{1}{2} \epsilon_a \sin 2\xi \frac{\partial^2 E_y}{\partial x^2} \\ & + (n_\perp^2 + \epsilon_a \sin^2 \xi) \frac{\partial^2 E_x}{\partial x^2} + n_\perp^2 \frac{\partial^2 E_x}{\partial y^2} + n_\perp^2 \frac{\partial^2 E_x}{\partial z^2} \\ & + \frac{1}{2} \epsilon_a \sin 2\xi \frac{\partial^2 E_x}{\partial x \partial y} \\ & = -k_0^2 n_\perp^2 \left[(n_\perp^2 + \epsilon_a \sin^2 \xi) E_x + \frac{1}{2} \epsilon_a \sin 2\xi E_y \right], \quad (6) \\ & \epsilon_a \sin^2 \xi \frac{\partial^2 E_x}{\partial x \partial y} + \frac{1}{2} \epsilon_a \sin 2\xi \frac{\partial^2 E_x}{\partial y^2} \\ & + (n_\parallel^2 - \epsilon_a \sin^2 \xi) \frac{\partial^2 E_y}{\partial y^2} + n_\perp^2 \frac{\partial^2 E_y}{\partial x^2} + n_\perp^2 \frac{\partial^2 E_y}{\partial z^2} \\ & + \frac{1}{2} \epsilon_a \sin 2\xi \frac{\partial^2 E_y}{\partial x \partial y} \\ & = -k_0^2 n_\perp^2 \left[(n_\parallel^2 - \epsilon_a \sin^2 \xi) E_y + \frac{1}{2} \epsilon_a \sin 2\xi E_x \right], \quad (7) \end{aligned}$$

$$K\nabla^2\xi + \frac{1}{4}\epsilon_0\epsilon_a[(|E_x|^2 - |E_y|^2) \sin 2\xi + (E_x E_y^* + E_x^* E_y) \cos 2\xi] = 0. \quad (8)$$

This system describing the evolution of the two, x and y , components of the electric field and the resulting director response is highly nonlinear in orientation ξ and not amenable to exact analysis. There are a number of dispersive terms in the equations for E_x and E_y which are small due to the factor ϵ_a and can be asymptotically simplified. A solitary wave stems from a balance between natural diffraction and effective self-focusing. Hence the system (6) and (7) can be simplified by balancing first-order diffraction, which is $O(1)$, and first-order nonlinearity, which is $O(\epsilon_a)$. In addition, the equations can be recast in paraxial form using

$$E_x = X e^{ik_0 n_\perp z}, \quad E_y = Y e^{ik_0 n_\parallel z}. \quad (9)$$

Taking the usual slowly varying approximation—in which $\partial^2 X/\partial z^2$ and $\partial^2 Y/\partial z^2$ are neglected—results in the paraxial equations

$$2ik_0 n_\perp \frac{\partial X}{\partial z} + \frac{\partial^2 X}{\partial x^2} + \frac{\partial^2 X}{\partial y^2} + k_0^2 \epsilon_a X \sin^2 \xi + \frac{1}{2} k_0^2 \epsilon_a Y e^{ik_0(n_\parallel - n_\perp)z} \sin 2\xi = 0, \quad (10)$$

$$2ik_0 n_\parallel \frac{\partial Y}{\partial z} + \frac{\partial^2 Y}{\partial x^2} + \frac{n_\parallel^2}{n_\perp^2} \frac{\partial^2 Y}{\partial y^2} - k_0^2 \epsilon_a Y \sin^2 \xi + \frac{1}{2} k_0^2 \epsilon_a X e^{-ik_0(n_\parallel - n_\perp)z} \sin 2\xi = 0, \quad (11)$$

$$K\nabla^2\xi + \frac{1}{4}\epsilon_0\epsilon_a[(|X|^2 - |Y|^2) \sin 2\xi + 2 \operatorname{Re}XY^* e^{-ik_0(n_\parallel - n_\perp)z} \cos 2\xi] = 0. \quad (12)$$

This intuitive compensation of leading-order diffraction and nonlinearity can be formalized through a coordinate scaling analysis. Due to ϵ_a being small, the x and y scales of the solitary wave are long. So we can set the long wave spatial scales as $\bar{x} = \sqrt{\epsilon_a}x$ and $\bar{y} = \sqrt{\epsilon_a}y$, with $\bar{z} = \epsilon_a z$. The full Eqs. (6)–(8) are then transformed to these new, slowly varying space variables. Keeping only the first-order, $O(1)$, terms and making the paraxial approximation (9) yields the Eqs. (10)–(12) [transformed back to (x, y, z) from $(\bar{x}, \bar{y}, \bar{z})$].

Moreover, the equations can be set in nondimensional form using the rescaled space variables

$$\bar{z} = \frac{k_0 \epsilon_a}{n_\perp} z, \quad \bar{x} = k_0 \sqrt{\epsilon_a} x, \quad \bar{y} = k_0 \sqrt{\epsilon_a} y. \quad (13)$$

These nondimensional variables are the long wave variables $(\bar{x}, \bar{y}, \bar{z})$ scaled by the wave number k_0 . The electric fields can be nondimensionalized on an input wave packet of power P_b , amplitude A_b , and width W_b , so that $E_x = A_b X$ and $E_y = A_b Y$. For a Gaussian beam, the amplitude scale A_b is determined from the power by

$$P_b = \frac{\pi}{2} C A_b^2 W_b^2, \quad C = \frac{1}{2} \epsilon_0 c n_e. \quad (14)$$

Applying this nondimensionalization, Eqs. (10)–(12) become

$$2i \frac{\partial X}{\partial \bar{z}} + \frac{\partial^2 X}{\partial \bar{x}^2} + \frac{\partial^2 X}{\partial \bar{y}^2} + X \sin^2 \xi + \frac{1}{2} Y e^{\frac{i\bar{z}}{1+\gamma}} \sin 2\xi = 0, \quad (15)$$

$$2i\gamma \frac{\partial Y}{\partial \bar{z}} + \frac{\partial^2 Y}{\partial \bar{x}^2} + \gamma^2 \frac{\partial^2 Y}{\partial \bar{y}^2} - Y \sin^2 \xi + \frac{1}{2} X e^{\frac{-i\bar{z}}{1+\gamma}} \sin 2\xi = 0, \quad (16)$$

$$v\nabla^2\xi + (|X|^2 - |Y|^2) \sin 2\xi + 2 \operatorname{Re}(XY^* e^{\frac{-i\bar{z}}{1+\gamma}}) \cos 2\xi = 0, \quad (17)$$

where

$$\gamma = \frac{n_\parallel}{n_\perp}, \quad v = \frac{4Kk_0^2}{\epsilon_0 A_b^2}. \quad (18)$$

These scalings, applied to the material and geometry outlined earlier, correspond to typical dimensionless nonlocality $v = 600$, anisotropy $\gamma = 1.13$, thickness $L = 200$, and input waists $w_{X0} = w_{Y0} = 12$, which are used to obtain the results presented in the following. The nondimensional Eqs. (15)–(17) have the Lagrangian formulation

$$L = i(X^* X_{\bar{z}} - X X_{\bar{z}}^*) - |X_{\bar{x}}|^2 - |X_{\bar{y}}|^2 + i\gamma(Y^* Y_{\bar{z}} - Y Y_{\bar{z}}^*) - |Y_{\bar{x}}|^2 - \gamma^2 |Y_{\bar{y}}|^2 - \frac{1}{2} v |\nabla \xi|^2 + \operatorname{Re}(XY^* e^{\frac{-i\bar{z}}{1+\gamma}}) \sin 2\xi + \sin^2 \xi (|X|^2 - |Y|^2). \quad (19)$$

Unfortunately, there are no known solitary wave solutions of the reduced system (15)–(17), as for the nematic equations [18]. In these cases, other than using numerical methods to find solitary wave solutions, variational approximations have proved to be useful and give results in good agreement with numerical and experimental results [7,18,59,60]. The Gaussian approximations

$$X = (a_X e^{-r^2/w_X^2} + ig_X) e^{i\sigma_X}, \\ Y = (a_Y e^{-r^2/w_Y^2} + ig_Y) e^{i\sigma_Y}, \\ \xi = \alpha e^{-r^2/\beta^2}, \quad (20)$$

with $r^2 = \bar{x}^2 + \bar{y}^2$, are appropriate for variational approximations to nematicons, where the parameters a_X , a_Y , w_X , w_Y , σ_X , σ_Y , α , β , g_X , and g_Y are functions of \bar{z} [18]. The trial functions for the electric fields X and Y have space independent terms ig_X and ig_Y . The beam components oscillate as they propagate, which generates diffractive radiation, forming a shelf under them [59]. These shelf terms ig_X and ig_Y represent the long-wavelength radiation produced in the vicinity of the beam, whose existence and spatially independent form was shown from the inverse scattering method applied to the NLS equation [59]. The shed radiation away from the beam is not dealt with here [59,60] as it has appreciable effects exclusively on long \bar{z} scales [60]. The radiation shelves under the beam can be assumed as circles of radii ℓ_X and ℓ_Y under X and Y , respectively [59,60]. Note that the inclusion of the radiation generated by the evolving beam is an alternative to the chirp method of Anderson [61].

Since the \bar{y} -component electric-field Eq. (16) has non-symmetric \bar{x} and \bar{y} diffraction coefficients, the trial function

for Y in (20) should have different widths in \tilde{x} and \tilde{y} , $w_{Y\tilde{x}}$ and $w_{Y\tilde{y}}$. Indeed, numerical solutions show that even if the initial components have a circular cross section, they evolve to an elliptic shape; see Fig. 2(g). Even though the trial functions (20) could be extended to have different widths $w_{X\tilde{x}}$ and $w_{X\tilde{y}}$ in \tilde{x} and \tilde{y} for X and, likewise, different $w_{Y\tilde{x}}$ and $w_{Y\tilde{y}}$ for Y , this would significantly increase the complexity of the resulting modulation equations, with only marginal changes in their solution as ϵ_a is small— $\gamma \sim 1$. Hence, for the sake of simplicity, the circular trial functions (20) will be employed in the following.

The trial functions (20) are substituted into the Lagrangian (19), which is then averaged by integrating in \tilde{x} and \tilde{y} from $-\infty$ to ∞ [2], noting that the beam parameters a_X , a_Y , w_X , w_Y , α , β , σ_X , and σ_Y depend on \tilde{z} . However, it is not possible to calculate the averaging integrals for the terms involving $\sin^2 \xi$ and $\sin 2\xi$ in (19), so another convenient assumption is that the director angle $|\xi|$ is small and the trigonometric functions can be expanded to their first terms in Taylor series. The resulting modulation equations provide solutions in good agreement with numerical integration of the full Eqs. (15)–(17). The averaged Lagrangian \mathcal{L} is then

$$\begin{aligned} \frac{1}{\pi} \mathcal{L} = & -(a_X^2 w_X^2 + 2\ell_X g_X^2) \sigma_X' + 2w_X^2 g_X a_X' \\ & + 4a_X w_X g_X w_X' - 2a_X w_X^2 g_X' - a_X^2 \\ & - \gamma (a_Y^2 w_Y^2 + 2\ell_Y g_Y^2) \sigma_Y' + 2\gamma w_Y^2 g_Y a_Y' \\ & + 4\gamma a_Y w_Y g_Y w_Y' - 2\gamma a_Y w_Y^2 g_Y' - \frac{1}{2} (1 + \gamma^2) a_Y^2 \\ & + \frac{2}{D} \alpha a_X a_Y w_X^2 w_Y^2 \beta^2 \cos \theta - \frac{1}{2} \nu \alpha^2 \\ & + \frac{1}{2} \alpha^2 \left[\frac{a_X^2 w_X^2 \beta^2}{\beta^2 + w_X^2} - \frac{a_Y^2 w_Y^2 \beta^2}{\beta^2 + w_Y^2} \right]. \end{aligned} \quad (21)$$

Here

$$D = \beta^2 w_X^2 + \beta^2 w_Y^2 + w_X^2 w_Y^2, \quad \theta = \frac{\tilde{z}}{1 + \gamma} - \sigma_X + \sigma_Y. \quad (22)$$

Taking variations of the above averaged Lagrangian with respect to all the parameters, except the director width β , gives the modulation equations

$$\frac{d}{d\tilde{z}} [a_X^2 w_X^2 + 2\ell_X^2 g_X^2] = -\frac{2\alpha a_X a_Y w_X^2 w_Y^2 \beta^2}{D} \sin \theta, \quad (23)$$

$$\gamma \frac{d}{d\tilde{z}} [a_Y^2 w_Y^2 + 2\ell_Y^2 g_Y^2] = \frac{2\alpha a_X a_Y w_X^2 w_Y^2 \beta^2}{D} \sin \theta, \quad (24)$$

$$\frac{d}{d\tilde{z}} a_X w_X^2 = \ell_X^2 g_X \frac{d\sigma_X}{d\tilde{z}}, \quad (25)$$

$$\frac{d}{d\tilde{z}} a_Y w_Y^2 = \ell_Y^2 g_Y \frac{d\sigma_Y}{d\tilde{z}}, \quad (26)$$

$$\frac{dg_X}{d\tilde{z}} = \frac{a_X}{2w_X^2} \quad (27)$$

$$\begin{aligned} & - \frac{2\alpha a_Y w_Y^2 \beta^2}{D^2} (w_X^2 \beta^2 - w_Y^2 \beta^2 + w_X^2 w_Y^2) \cos \theta, \\ & \gamma \frac{dg_Y}{d\tilde{z}} = \frac{(1 + \gamma^2) a_Y}{4w_Y^2} \end{aligned} \quad (28)$$

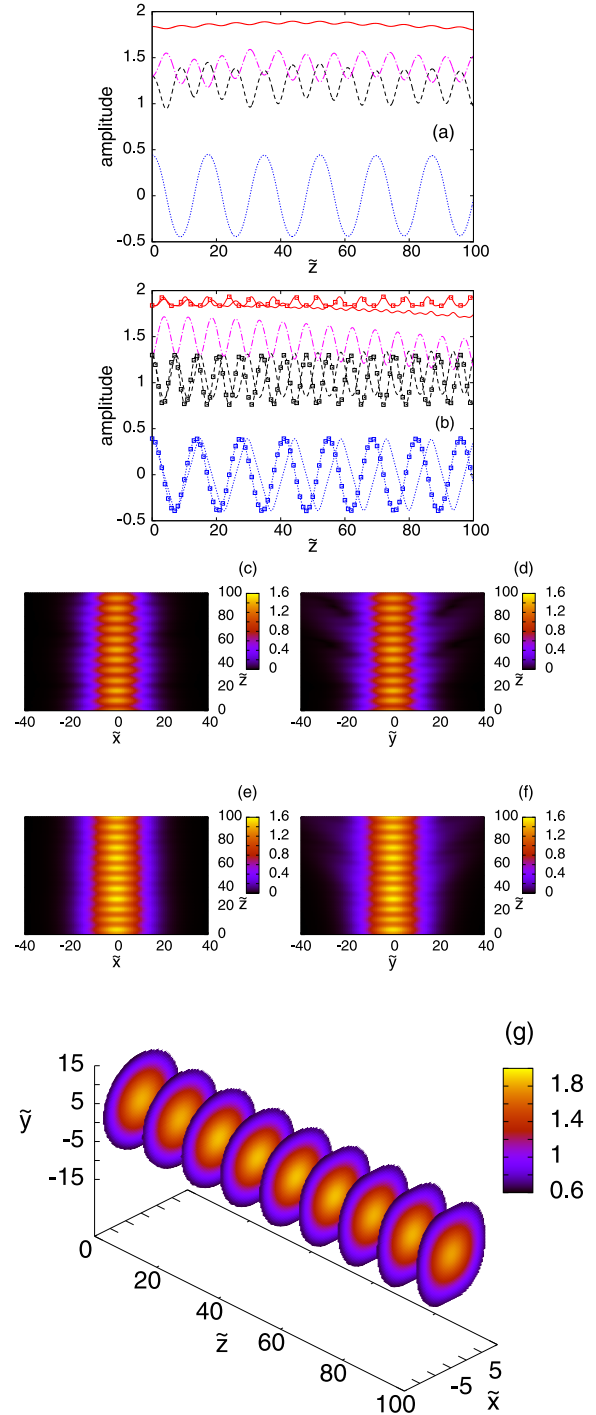


FIG. 2. Evolution of beam and transverse director orientation for an in-phase initial excitation with $a_{X0} = a_{Y0} = 1.3$ and $\sigma_{X0} = \sigma_{Y0} = 0$. (a) Numerical solution of Eqs. (15)–(17) versus z . Red (solid) line: total amplitude a_b ; black (dashed) line: amplitude a_X of X ; pink (dashed) line: amplitude a_Y of Y ; blue (dotted) line: director angle amplitude α , (b) same as (a), but for solution of the full modulation Eqs. (23)–(31) with same line types. Lines with symbols: solution (32)–(36) of the approximate modulation equations; (c) numerical X evolution through $\tilde{y} = 0$, (d) numerical X evolution through $\tilde{x} = 0$, (e) numerical Y evolution through $\tilde{y} = 0$, (f) numerical Y evolution through $\tilde{x} = 0$, and (g) color plot of beam intensity cross sections $\sqrt{|X|^2 + |Y|^2}$ calculated numerically at fixed propagation intervals.

$$\begin{aligned}
& - \frac{2\alpha a_X w_X^2 \beta^2}{D^2} (w_Y^2 \beta^2 - w_X^2 \beta^2 + w_X^2 w_Y^2) \cos \theta, \\
& \frac{d\sigma_X}{d\tilde{z}} = \frac{-2}{w_X^2} + \frac{2\alpha a_Y w_X^2 w_Y^2 \beta^2}{a_X D^2} (\beta^2 + w_X^2) \cos \theta, \quad (29) \\
& \gamma \frac{d\sigma_Y}{d\tilde{z}} = -\frac{1 + \gamma^2}{w_Y^2} + \frac{2\alpha a_X w_X^2 w_Y^2 \beta^2}{a_Y D^2} (\beta^2 + w_Y^2) \cos \theta, \quad (30)
\end{aligned}$$

plus the algebraic equation

$$\alpha = \frac{2a_X a_Y w_X^2 w_Y^2 \beta^2 \cos \theta}{D[v - \beta^2 \Delta]}, \quad \Delta = \frac{a_X^2 w_X^2}{\beta^2 + w_X^2} - \frac{a_Y^2 w_Y^2}{\beta^2 + w_Y^2}, \quad (31)$$

for the amplitude of the director (re)orientation. In principle, these equations are completed by taking variations of the averaged Lagrangian with respect to β in order to determine the width of the director reorientation. However, away from the components X and Y , the solution of the director Eq. (17) varies as $\ln r$, which is one of the homogeneous solutions of Laplace's equation. This means that the appropriate width of the director response is not that given by the variational equation for β , as the trial function for the director is based on a Gaussian, but the thickness L of the NLC cell. We then set $\beta = L/(2\sqrt{\ln 100})$, so that the angular director response (20) falls to 0.01 of its value in the center and the boundary condition is approximately satisfied. It should be stressed again that the results do not depend significantly on this approximation to the boundary condition. In previous applications of this Lagrangian technique, the director distribution decayed exponentially away from the beam due to the director being pretilted by an external electric field, so that the boundary condition was automatically satisfied [18,60]. The trial function (20) for ξ then represents the director distribution directly forced by the beam. However, it does not include the $\ln r$ behavior away from the beam, because owing to the exponential decay this contributes negligibly to the beam-director interaction when averaging the Lagrangian (19).

The modulation Eqs. (23) and (24) model the power of the components X and Y . Adding them shows that the total light power is conserved, although the power cycles between the two components, causing them to oscillate in amplitude and width. The inclusion of the radiation shelf, the g_X and g_Y terms in the trial functions (20), is vital to obtaining consistent modulation equations which yield physical results and agree with numerical solutions. By neglecting the radiation shelf and setting $g_X = 0$ and $g_Y = 0$ in Eqs. (27) and (28), when α is substituted from (31), these modulation equations would become singular for $\cos \theta = 0$. The circulating radiation into and out of the shelf as the beam evolves stops this unphysical singularity and causes the amplitudes and widths to oscillate between nonzero limits, in agreement with numerical solutions. The final quantities to be determined are the shelf radii ℓ_X and ℓ_Y , evaluated by matching the solitary wave phase to the oscillation period of the modulation equations around their fixed point [59,60]. However, this leads to highly involved expressions. As the shelf radii are proportional to the widths w_X and w_Y [59,60], we picked the pertinent factor to match modulation and numerical solutions for a particular parameter

choice and then fixed it for all other solutions [62,63]. We thus set the values $\ell_X = 0.3w_X$ and $\ell_Y = 0.3w_Y$.

In general, the modulation Eqs. (23)–(31) need to be solved numerically. If the oscillations in the components are small, little radiation is fed into the shelves under the beam and $|g_X|$ and $|g_Y|$ can be assumed small, as well [7,59,60]. In this case, Eqs. (23)–(31) can be solved to yield, to $O(|\alpha|)$,

$$\begin{aligned}
a_X &= a_{X0} - \frac{a_{X0} a_{Y0}^2 w_{X0}^2 w_{Y0}^4 \beta^4}{D_0^2 \psi(v - \beta^2 \Delta_0)} [\cos 2(\psi \tilde{z} - \sigma_{X0} + \sigma_{Y0}) \\
&\quad - \cos 2(\sigma_{X0} - \sigma_{Y0})], \quad (32)
\end{aligned}$$

$$\begin{aligned}
a_Y &= a_{Y0} + \frac{a_{X0}^2 a_{Y0} w_{X0}^4 w_{Y0}^2 \beta^4}{\gamma D_0^2 \psi(v - \beta^2 \Delta_0)} [\cos 2(\psi \tilde{z} - \sigma_{X0} + \sigma_{Y0}) \\
&\quad - \cos 2(\sigma_{X0} - \sigma_{Y0})], \quad (33)
\end{aligned}$$

$$\begin{aligned}
w_X &= w_{X0} + \frac{a_{Y0}^2 w_{X0}^3 w_{Y0}^4 \beta^4}{2D_0^2 \psi(v - \beta^2 \Delta_0)} [\cos 2(\psi \tilde{z} - \sigma_{X0} + \sigma_{Y0}) \\
&\quad - \cos 2(\sigma_{X0} - \sigma_{Y0})], \quad (34)
\end{aligned}$$

$$\begin{aligned}
w_Y &= w_{Y0} - \frac{a_{X0}^2 w_{X0}^4 w_{Y0}^3 \beta^4}{2\gamma D_0^2 \psi(v - \beta^2 \Delta_0)} [\cos 2(\psi \tilde{z} - \sigma_{X0} + \sigma_{Y0}) \\
&\quad - \cos 2(\sigma_{X0} - \sigma_{Y0})], \quad (35)
\end{aligned}$$

$$\alpha = \frac{2a_{X0} a_{Y0} w_{X0}^2 w_{Y0}^2 \beta^2}{D_0(v - \beta^2 \Delta_0)} \cos(\psi \tilde{z} - \sigma_{X0} + \sigma_{Y0}), \quad (36)$$

where

$$\psi = \frac{1}{1 + \gamma} + \frac{2}{w_{X0}^2} - \frac{1 + \gamma^2}{\gamma w_{Y0}^2}. \quad (37)$$

The subscript 0 denotes quantities at $\tilde{z} = 0$. This approximation agrees well with numerical solutions, as long as the components do not evolve far from their initial state. It shows that the only effect of an initial phase difference between X and Y is a shift of their oscillations and the director oscillation, without changes in amplitudes and periods. These basic findings for the evolution of beam and director reorientation based on modulation theory will be confirmed below through comparisons with numerical solutions of the paraxial Eqs. (15)–(17).

IV. RESULTS AND DISCUSSION

Figure 2 shows a set of results for equal amplitude, in-phase input components X and Y , comparing full numerical solutions of Eqs. (15)–(17) with those of the modulation Eqs. (23)–(31) and the approximate solutions (32)–(36). This case corresponds to a linearly polarized input beam, with electric field initially oscillating at $\pi/4$ in the plane (\tilde{x}, \tilde{y}) and therefore producing a strong nonlinear response [14], at variance with purely extraordinary (ordinary) waves polarized along \tilde{y} (\tilde{x}), as they induce no reorientation based on Eq. (1) below the Fréedericks threshold [13]. The initial conditions for X and Y are the trial functions (20) and the amplitudes a_X , a_Y and widths w_X , w_Y chosen so that the beam amplitude $|(X, Y)|$ undergoes minimal adjustments down the NLC sample. Figures 2(a) and 2(b) show the total beam

amplitude a_b , the amplitudes of its \tilde{x} and \tilde{y} components, and the amplitude of the director reorientation, respectively. The various solutions show substantial agreement of theory and numerics despite the approximations, even though some small discrepancies are visible, particularly in the detailed evolution of the amplitudes and the periodicity of the nonlinear director modulation. The inherent physics, stemming from a periodic orientation of the optic axis in the transverse plane (\tilde{x} , \tilde{y}) about its initial alignment along \tilde{y} , with the geometric phase yielding phase front curvature and self-focusing, emerges clearly from the model. The role of the geometric phase, previously described by polarimetry and the Poincaré sphere using the Jones calculus and the Stokes parameters (see Refs. [64–66] and references therein), is clearly manifested through the evolution of beam size and amplitude owing to self-trapping. The solitary wave is transversely confined despite propagation in a uniform index environment and, as pointed out for the 1D case in Ref. [51], it oscillates in width and amplitude versus \tilde{z} [Figs. 2(c)–2(f)] owing to the phase velocity mismatch between eigenpolarizations (birefringence). The beam intensity evolves to an elliptic cross section owing to the lack of circular symmetry around \tilde{z} [Fig. 2(g)].

The full modulation solution for the overall amplitude is in excellent agreement with the numerical result, including the slight decay versus \tilde{z} . The approximate modulation solution (32)–(36) agrees well also, but it oscillates about the initial amplitude without the slight decay versus \tilde{z} . The agreement between X and Y amplitudes given by the numerical and modulation solutions is also satisfactory, although the modulation amplitude has larger oscillations. The full and approximate modulation solutions for X and for Y match quite well; the curves for Y are not displayed to avoid cluttering Fig. 2(b). The amplitude of the director oscillation is correctly predicted by the modulation theory, with the modulation period slightly shorter than the numerical one.

Figures 2(c)–2(g) display cross sections of each evolving component and snapshots of the beam intensity. In Fig. 2(g) we plotted values for which $\sqrt{|X|^2 + |Y|^2} \geq 0.5\sqrt{a_X^2 + a_Y^2}$. Out of phase oscillations of the amplitudes and widths of X and Y can be appreciated, as predicted by the modulation theory, while the beam evolves from its initially circular profile to an elliptic shape with the major axis in the \tilde{y} direction. This can be attributed to the \tilde{y} diffraction coefficient γ^2 in Eq. (16) being different to that for X [Eq. (15)]. This, discussed above for the choice of the trial functions for X and Y , suggests that the \tilde{y} width of Y should be $\gamma = n_{\parallel}/n_{\perp} = 1.13$ times that of X . The ratio of the numerical \tilde{y} widths of Y and X oscillates between 0.96 and 1.22 during propagation, in agreement with theory. In addition, the ratio of the \tilde{y} and \tilde{x} widths of the total beam (X, Y) in Fig. 2(g) monotonically increases to 1.16 at $\tilde{z} = 100$.

Figure 3 displays similar results as in Fig. 2, but for an initial phase difference of π between components, i.e., a linear input polarization with electric field at $-\pi/4$. Consistent with the inherent physics of the all-optical reorientation of neutral molecules, the approximate modulation solution (32)–(36) predicts that the amplitudes and widths evolve in an identical manner to that for the in-phase components, with the director oscillations simply shifted by π . This is borne out by the numerical solutions in Figs. 3(a) and 3(c)–3(f). The equivalent

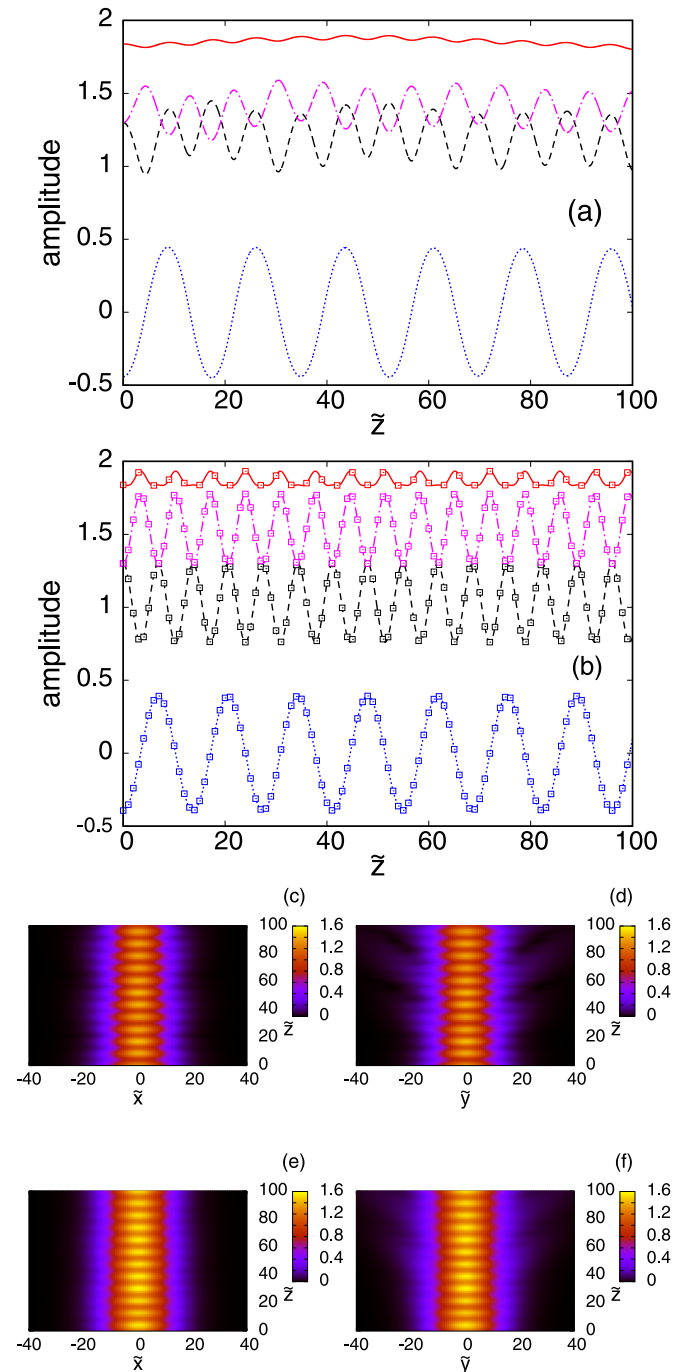


FIG. 3. Evolution of beam and transverse orientation of optic axis for an excitation with $a_{X0} = a_{Y0} = 1.3$, $w_{X0} = w_{Y0} = 12$, $\sigma_{X0} = -\pi$, and $\sigma_{Y0} = 0$. (a) Numerical solution of Eqs. (15)–(17) versus z . Red (solid) line: total amplitude a_b ; black (dashed) line: amplitude a_X of X ; pink (dashed) line: amplitude a_Y of Y ; blue (dotted) line: director amplitude α , (b) same as (a), but for approximate solution (32)–(36) of modulation equations, (c) numerical X evolution through $\tilde{y} = 0$, (d) numerical X evolution through $\tilde{x} = 0$, (e) numerical Y evolution through $\tilde{y} = 0$, and (f) numerical Y evolution through $\tilde{x} = 0$.

of the beam evolution in Fig. 2(g) is redundant and is not displayed.

Figure 4 presents solutions and comparisons for an initial phase difference of $\pi/2$, i.e., a circularly polarized input. The

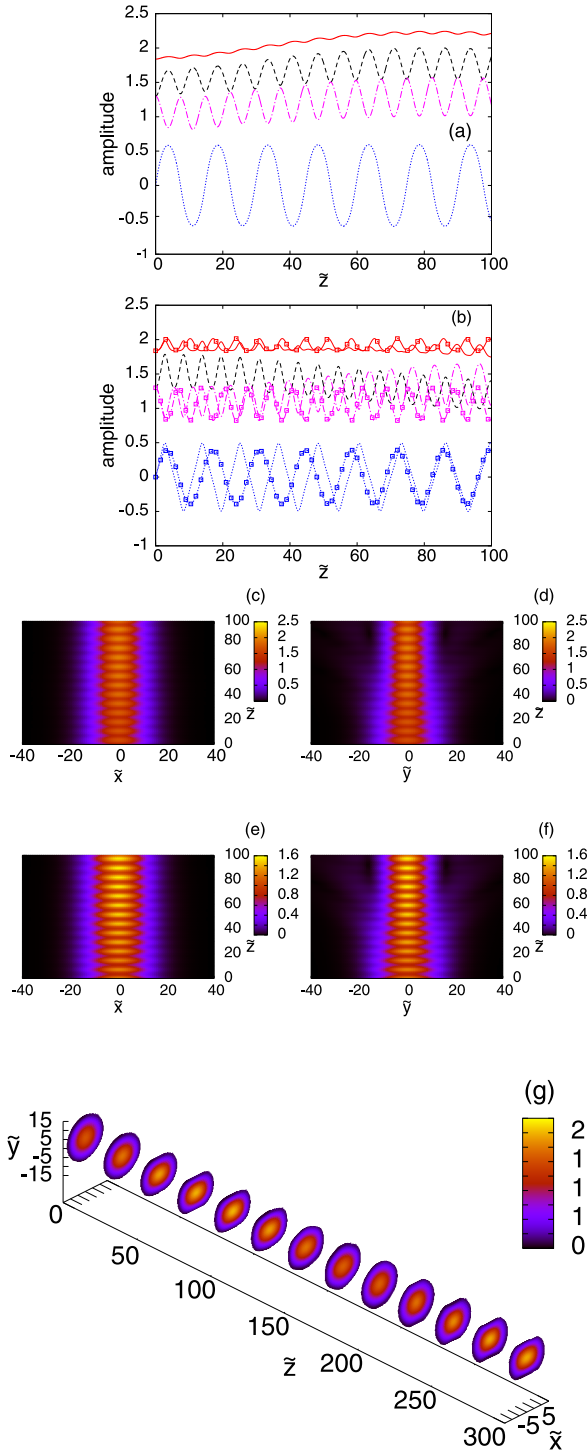


FIG. 4. Evolution of beam and transverse director orientation for an initial excitation with $a_{X0} = a_{Y0} = 1.3$, $\sigma_{X0} = \pi/2$, and $\sigma_{Y0} = 0$. (a) Numerical solution of Eqs. (15)–(17) versus z . Red (solid) line: total amplitude a_b ; black (dashed) line: amplitude a_X of X ; pink (dashed) line: amplitude a_Y of Y ; blue (dotted) line: director orientation amplitude α , (b) same as (a), but for solution of the full modulation equations (23)–(31) with the same line types. Lines with symbols: solution (32)–(36) of the approximate modulation equations, (c) numerical X evolution through $\bar{y} = 0$, (d) numerical X evolution through $\bar{x} = 0$, (e) numerical Y evolution through $\bar{y} = 0$, (f) numerical Y evolution through $\bar{x} = 0$, and (g) color plot of beam intensity cross sections at fixed propagation intervals.

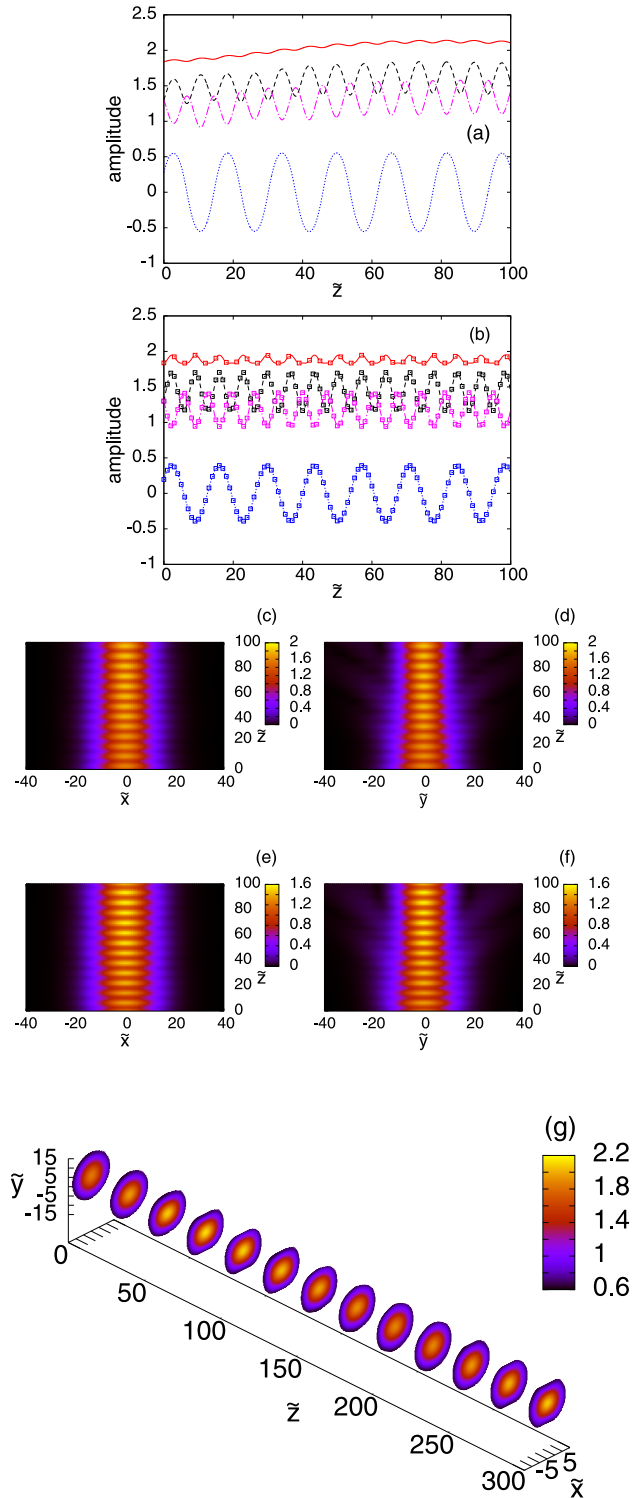


FIG. 5. Evolution of beam and transverse director orientation for an input excitation with $a_{X0} = a_{Y0} = 1.3$, $\sigma_{X0} = \pi/3$, and $\sigma_{Y0} = 0$. (a) Numerical solution of Eqs. (15)–(17) versus z . Red (solid) line: total amplitude a_b ; black (dashed) line: amplitude a_X of X ; pink (dashed) line: amplitude a_Y of Y ; blue (dotted) line: director angle amplitude α , (b) same as (a), but for approximate solution (32)–(36), (c) numerical X evolution through $\bar{y} = 0$, (d) numerical X evolution through $\bar{x} = 0$, (e) numerical Y evolution through $\bar{y} = 0$, (f) numerical Y evolution through $\bar{x} = 0$, and (g) color plot of beam intensity cross sections at fixed propagation intervals.

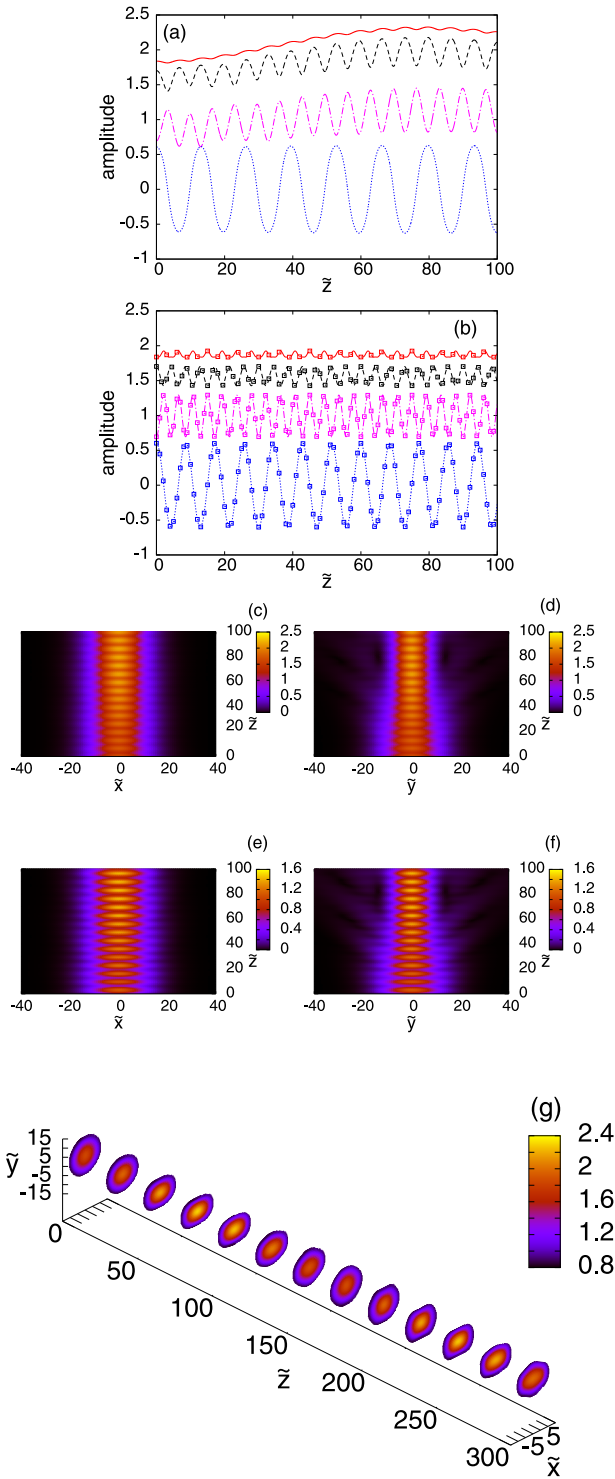


FIG. 6. Evolution of beam and transverse director orientation for an initial excitation with in-phase components $\sigma_{X0} = \sigma_{Y0} = 0$ and $a_{X0} = 1.7$, $a_{Y0} = 0.7$. (a) Numerical solution of Eqs. (15)–(17) versus z . Red (solid) line: total amplitude a_b ; black (dashed) line: amplitude a_X of X ; pink (dashed) line: amplitude a_Y of Y ; blue (dotted) line: director angle amplitude α , (b) same as (a), but for approximate solution (32)–(36) of modulation equations, (c) numerical X evolution through $\tilde{y} = 0$, (d) numerical X evolution through $\tilde{x} = 0$, (e) numerical Y evolution through $\tilde{y} = 0$, (f) numerical Y evolution through $\tilde{x} = 0$, and (g) color plot of beam intensity cross section at fixed propagation intervals.

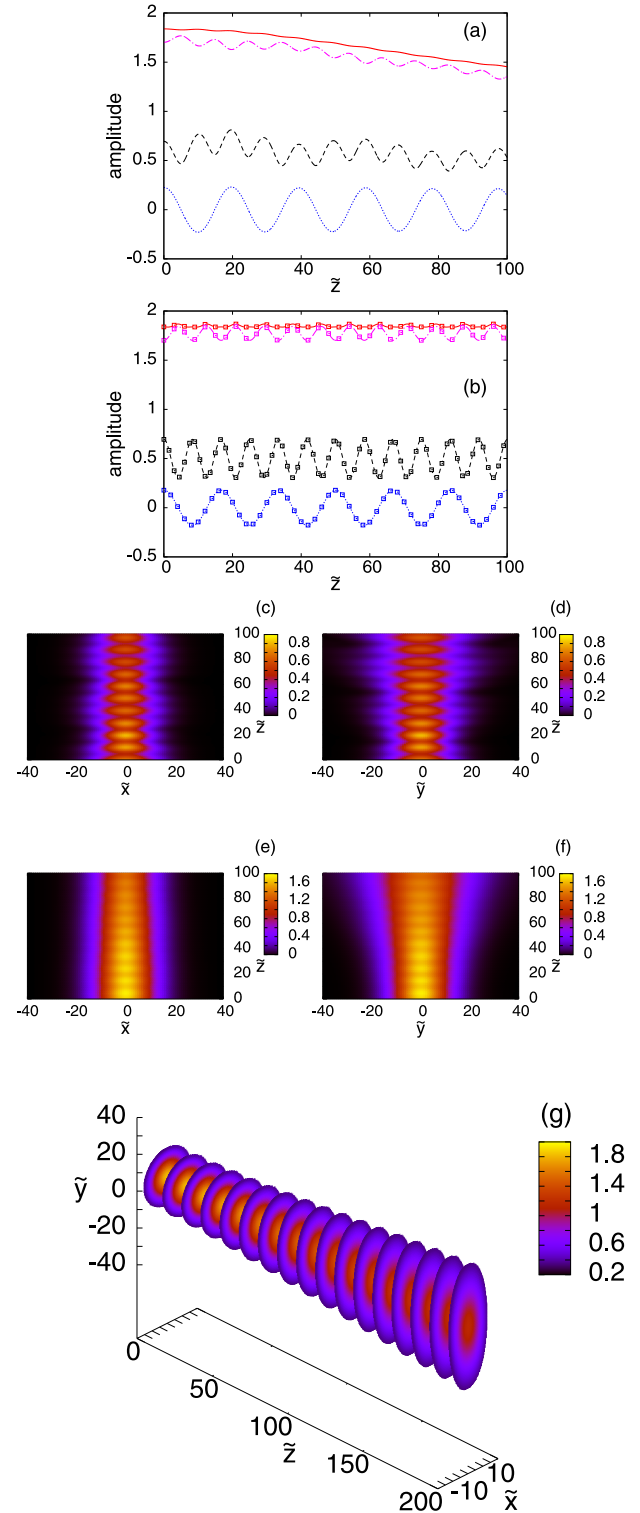


FIG. 7. Evolution of beam and transverse director orientation for an initial excitation with in-phase components $\sigma_{X0} = \sigma_{Y0} = 0$ and $a_{X0} = 0.7$, $a_{Y0} = 1.7$. (a) Numerical solution of (15)–(17) versus z . Red (solid) line: total amplitude a_b ; black (dashed) line: amplitude a_X of X ; pink (dashed) line: amplitude a_Y of Y ; blue (dotted) line: director amplitude α , (b) same as (a), but for approximate solution (32)–(36), (c) numerical X evolution through $\tilde{y} = 0$, (d) numerical X evolution through $\tilde{x} = 0$, (e) numerical Y evolution through $\tilde{y} = 0$, (f) numerical Y evolution through $\tilde{x} = 0$, and (g) color plot of beam intensity cross section at fixed propagation intervals.

numerical solutions show that the total beam amplitude a_b and the component amplitudes a_X and a_Y slightly increase versus \tilde{z} ; the director oscillates uniformly with the same amplitude as in Fig. 2 and Fig. 3. The amplitude trend can be explained from panels (c)–(f), showing that X and Y have constant \tilde{x} widths, but a contraction in the \tilde{y} widths, which translates into an amplitude growth due to power conservation. This asymmetric evolution of the profile can also be observed in Fig. 4(g) calculated up to $\tilde{z} = 300$. The total beam profile oscillates as the beam propagates down the cell. The beam initially contracts across \tilde{y} and becomes distinctly elliptical, but the \tilde{y} width then expands again, with this process repeating so that the beam ellipticity oscillates down the cell. The \tilde{y} widths of X and Y in Figs. 4(d) and 4(f) mirror this elliptical evolution of the profile. As for the in-phase (and π out-of-phase) field inputs, the approximate and full solutions of the modulation equations are in good agreement, with some deviation versus \tilde{z} , as expected. The modulation solution Y has a rise in amplitude similar to the numerical solution, while the X amplitude decreases, resulting in a nearly constant total amplitude.

Figure 5 presents the solutions for a $\pi/3$ initial phase difference. The results are similar to those for the $\pi/2$ phase case (Fig. 4), except for the expected initial translation of the director modulation and the details of the evolution. In particular, the beam cross section again oscillates in ellipticity as the beam propagates down the cell. The solutions of the full modulation equations are not shown for the sake of visual clarity.

Finally, we studied the formation of spin-optical solitons with the input consisting of in-phase components, of equal profile and waists, but power imbalanced by a factor of 6. The latter was arbitrarily chosen to provide a substantial intensity mismatch. Figure 6 shows the results for an input with \tilde{x} and \tilde{y} component powers in the ratio 6:1. As the X field is stronger than the Y and the input is linearly polarized, strong reorientation of the optic axis occurs and affects the polarization evolution, i.e., the resulting geometric phase. The spin-orbit interaction produces more marked self-focusing of both components across \tilde{y} , as visible in Figs. 6(d) and 6(f). Noteworthy is that the solitary profile assumes an elliptical shape with a periodic evolution in ellipticity, as seen in Fig. 6(g), over an extended propagation distance, as noted for the $\pi/2$ and $\pi/3$ phase differences for components of equal power.

An opposite trend can be observed in Fig. 7 for the formation of spin-optical solitons when the input components are in phase, but with powers mismatched in the ratio 1:6, i.e., with Y larger than X . Nonlinear reorientation is substantially reduced in amplitude and period, both for the numerical and modulation solutions [see Figs. 7(a) and 7(b)]. Correspondingly, the numerical amplitudes tend to decay because self-focusing is weaker, as can be observed in Figs. 7(c)–7(f). Also, the solitary wave profile assumes a distinctly elliptical shape with a periodic evolution in ellipticity, as visible in Fig. 7(g) over $\tilde{z} = 200$. The ratio of the \tilde{y} widths of the Y and X components oscillates between 0.98 and 1.33, i.e., around the theoretical value $\gamma = n_{\parallel}/n_{\perp} = 1.13$. In contrast

to the equal component power cases, however, the ratio of the \tilde{y} and \tilde{x} widths of the total beam (X, Y) in Fig. 7(g) grows monotonically from 1 at $\tilde{z} = 0$ to 2.69 at $\tilde{z} = 200$. The evolution of profile ellipticity is a remarkably peculiar feature of these spin-optical solitons, deserving further investigation.

V. CONCLUSIONS

Spin-orbit interactions of light in optically anisotropic dielectric media encompass a wealth of effects and phenomena. When all-optical reorientation is available, as in nematic liquid crystals, nonlinear periodic changes in transverse orientation of the optic axis, together with the accumulation of a geometric Pancharatnam-Berry phase stemming from point-to-point beam polarization evolution, can lead to self-confinement and spatial solitary waves even in the absence of changes in refractive indices. It is worth noting that spin-optical solitons stemming from nonlinearity and nonuniform changes in polarization state recall the “quadratic cascading” which occurs in parametric optical interactions, for which velocity mismatched fundamental and generated frequency components exchange energy in a periodic fashion, while acquiring a net relative phase. Even though after a period (beat length) all the energy can be retrieved back at the initial frequencies, the pointwise (amplitude dependent) nonlinear distortion of the phase front can lead to transverse confinement and the formation of quadratic solitons (or “simultons”) with no associated refractive index waveguides [3,57,58,67–69]. An in-depth study of the formal connection between such rather diverse nonlinear mechanisms is worth pursuing, as a wealth of other physical effects could benefit from the gained understanding, both in terms of models, numerical techniques and solutions, and the role of physical features, particularly nonlocality and periodicity. We have numerically and theoretically investigated spin-optical solitons in nematic liquid crystals, studying a planar configuration with purely transverse orientation of the molecular director with respect to the propagating beam wave vector. Spin-optical solitons are self-confined solutions connected with a longitudinally modulated orientation of the symmetry axis: they exhibit periodically evolving polarization state, widths and peak amplitudes, and profile ellipticity, for all the investigated input configurations at normal incidence, including relative phase and amplitudes. Self-confinement is weakly dependent on the initial polarization state, except for those cases in which either nonlinear reorientation does not take place (pure extraordinary or ordinary eigenwaves) or is weakly effective (stronger field component along the optic axis at rest). Other peculiar features of these PB-phase solitons include a transverse profile with elliptical shape and varying ellipticity, which will be analyzed and discussed in a forthcoming publication with reference to both field components. In addition, the role of longitudinal nonlocality in the medium needs be addressed, as it is expected to affect the response to light beams and their polarization state evolution, intervening on some of the features of these fascinating spin-optical solitons.

- [1] R. Y. Chiao, E. Garmire, and C. H. Townes, Self Trapping of Optical Beams, *Phys. Rev. Lett.* **13**, 479 (1964).
- [2] G. B. Whitham, *Linear and Nonlinear Waves* (J. Wiley and Sons, New York, 1974).
- [3] G. Assanto and G. I. Stegeman, Simple physics of quadratic spatial solitons, *Opt. Express* **10**, 388 (2002).
- [4] N. N. Akhmediev, Spatial solitons in Kerr and Kerr-like media, *Opt. Quantum Electron.* **30**, 535 (1998).
- [5] *Spatial Solitons*, edited by S. Trillo and W. Torruellas (Springer-Verlag, Heidelberg, 2001).
- [6] *Optical Solitons: From Fibers to Photonic Crystals*, edited by Y. S. Kivshar and G. Agrawal (Academic Press, San Diego, 2003).
- [7] *Nematicons*, edited by G. Assanto (John Wiley & Sons, Hoboken, 2012).
- [8] S. Skupin, O. Bang, D. Edmundson, and W. Krolikowski, Stability of two-dimensional spatial solitons in nonlocal nonlinear media, *Phys. Rev. E* **73**, 066603 (2006).
- [9] G. I. Stegeman and R. Stegeman, *Nonlinear Optics: Phenomena, Materials and Devices* (John Wiley & Sons, Hoboken, 2012).
- [10] N. F. Smyth, A. Piccardi, A. Alberucci, and G. Assanto, Highly nonlocal optical response: Benefit or drawback? *J. Nonlin. Opt. Phys. Mater.* **25**, 1650043 (2017).
- [11] G. I. Stegeman and M. Segev, Optical spatial solitons and their interactions: Universality and diversity, *Science* **286**, 1518 (1999).
- [12] I. C. Khoo, Nonlinear optics of liquid crystalline materials, *Phys. Rep.* **471**, 221 (2009).
- [13] N. V. Tabiryan, A. V. Sukhov, and B. Ya. Zel'dovich, Orientational optical nonlinearity of liquid crystals, *Mol. Cryst. Liq. Cryst.* **136**, 1 (1986).
- [14] G. Assanto and M. Peccianti, Spatial solitons in nematic liquid crystals, *IEEE J. Quantum Electron.* **39**, 13 (2003).
- [15] M. Peccianti and G. Assanto, Nematicons, *Phys. Rep.* **516**, 147 (2012).
- [16] G. Assanto and M. Karpierz, Nematicons: self-localized beams in nematic liquid crystals, *Liq. Cryst.* **36**, 1161 (2009).
- [17] G. Assanto, Nematicons: reorientational solitons from optics to photonics, *Liq. Cryst. Rev.* **6**, 170 (2018).
- [18] G. Assanto and N. F. Smyth, Self confined light waves in nematic liquid crystals, *Physica D: Nonlin. Phenom.* **402**, 132182 (2020).
- [19] J. M. L. MacNeil, N. F. Smyth, and G. Assanto, Exact and approximate solutions for optical solitary waves in nematic liquid crystals, *Physica D* **284**, 1 (2014).
- [20] N. Kravets, A. Piccardi, A. Alberucci, O. Buchnev, M. Kaczmarek, and G. Assanto, Bistability with Optical Beams Propagating in a Reorientational Medium, *Phys. Rev. Lett.* **113**, 023901 (2014).
- [21] A. Alberucci, A. Piccardi, N. Kravets, O. Buchnev, and G. Assanto, Soliton enhancement of spontaneous symmetry breaking, *Optica* **2**, 783 (2015).
- [22] M. Peccianti, A. Pasquazi, G. Assanto, and R. Morandotti, Enhancement of third harmonic generation in nonlocal spatial solitons, *Opt. Lett.* **35**, 3342 (2010).
- [23] I. B. Burgess, M. Peccianti, G. Assanto, and R. Morandotti, Accessible Light Bullets via Synergetic Nonlinearities, *Phys. Rev. Lett.* **102**, 203903 (2009).
- [24] U. A. Laudyn, M. Kwasny, A. Piccardi, M. Karpierz, R. Dabrowski, O. Chojnowska, A. Alberucci, and G. Assanto, Nonlinear competition in nematicon propagation, *Opt. Lett.* **40**, 5235 (2015).
- [25] K. Cyprych, P. S. Jung, Y. V. Izdebskaya, V. Shvedov, D. N. Christodoulides, and W. Krolikowski, Anomalous interaction of spatial solitons in nematic liquid crystals, *Opt. Lett.* **44**, 267 (2019).
- [26] S. Perumbilavil, A. Piccardi, R. Barboza, O. Buchnev, G. Strangi, M. Kauranen, and G. Assanto, Beaming random lasers with soliton control, *Nat. Commun.* **9**, 3863 (2018).
- [27] S. Perumbilavil, A. Piccardi, O. Buchnev, G. Strangi, M. Kauranen, and G. Assanto, Spatial solitons to mold random lasers in nematic liquid crystals, *Opt. Mater. Express* **8**, 3864 (2018).
- [28] M. Peccianti, C. Conti, G. Assanto, A. De Luca, and C. Umeton, Routing of anisotropic spatial solitons and modulational instability in liquid crystals, *Nature (London)* **432**, 733 (2004).
- [29] Y. V. Izdebskaya, Routing of spatial solitons by interaction with rod microelectrodes, *Opt. Lett.* **39**, 1681 (2014).
- [30] A. Alberucci, A. Piccardi, U. Bortolozzo, S. Residori, and G. Assanto, Nematicon all-optical control in liquid crystal light valves, *Opt. Lett.* **35**, 390 (2010).
- [31] A. Piccardi, A. Alberucci, U. Bortolozzo, S. Residori, and G. Assanto, Readdressable interconnects with spatial soliton waveguides in liquid crystal light valves, *IEEE Photon. Technol. Lett.* **22**, 694 (2010).
- [32] Y. V. Izdebskaya, V. Shvedov, G. Assanto, and W. Krolikowski, Magnetic routing of light-induced waveguides, *Nat. Commun.* **8**, 14452 (2017).
- [33] V. Shvedov, Y. V. Izdebskaya, Y. Sheng, and W. Krolikowski, Magnetically controlled negative refraction of solitons in liquid crystals, *Appl. Phys. Lett.* **110**, 091107 (2017).
- [34] S. Perumbilavil, M. Kauranen, and G. Assanto, Magnetic steering of beam-confined random laser in liquid crystals, *Appl. Phys. Lett.* **113**, 121107 (2018).
- [35] S. Pancharatnam, Generalized theory of interference, and its applications, *Proc. Indian Acad. Sci.* **44**, 398 (1956).
- [36] M. V. Berry, Quantal phase factors accompanying adiabatic changes, *Proc. R. Soc. A* **392**, 45 (1984).
- [37] S. M. Rytov, On the transition from wave to geometrical optics, *Dokl. Akad. Nauk. SSSR* **18**, 263 (1938).
- [38] K. Y. Bliokh, F. J. Rodríguez Fortuño, F. Nori, and A. V. Zayats, Spin-orbit interactions of light, *Nat. Photon.* **9**, 796 (2015).
- [39] Y. Ben Aryeh, Berry and Pancharatnam topological phases of atomic and optical systems, *J. Opt. B: Quantum Semiclass. Opt.* **6**, R1 (2004).
- [40] A. Ya. Bekshaev, Spin orbit interaction of light and diffraction of polarized beams, *J. Opt.* **19**, 085602 (2017).
- [41] C. T. Samlan, Spin-orbit interaction of light: The role of Pancharatnam-Berry phase, Ph.D. thesis, University of Hyderabad, 2017.
- [42] E. Bortolotti, Memories and notes presented by fellows, *Rend. R. Acc. Naz. Linc.* **4**, 552 (1926).
- [43] E. Hasman, G. Biener, A. Niv, and V. Kleiner, Space-variant polarization manipulation in inhomogeneous anisotropic media, *Prog. Opt.* **47**, 215 (2005).
- [44] L. Marrucci, C. Manzo, and D. Paparo, Optical Spin-to-Orbital Angular Momentum Conversion in Inhomogeneous Anisotropic Media, *Phys. Rev. Lett.* **96**, 163905 (2006).

- [45] E. Brasselet, Y. V. Izdebskaya, V. Shvedov, A. S. Desyatnikov, W. Krolikowski, and Yu. S. Kivshar, Dynamics of optical spin-orbit coupling in uniaxial crystals, *Opt. Lett.* **34**, 1021 (2009).
- [46] F. Cardano and L. Marrucci, Spin-orbit photonics, *Nat. Photon.* **9**, 776 (2015).
- [47] S. Slussarenko, A. Alberucci, C. P. Jisha, P. Piccirillo, E. Santamato, G. Assanto, and L. Marrucci, Guiding light via geometric phases, *Nat. Photon.* **10**, 571 (2016).
- [48] A. Alberucci, C. P. Jisha, L. Marrucci, and G. Assanto, Electromagnetic confinement via spin-orbit interaction in anisotropic dielectrics, *ACS Photon.* **3**, 2249 (2016).
- [49] C. P. Jisha, A. Alberucci, L. Marrucci, and G. Assanto, Interplay between diffraction and the Pancharatnam-Berry phase in inhomogeneously twisted anisotropic media, *Phys. Rev. A* **95**, 023823 (2017).
- [50] M. A. Karpierz, M. Sierakowski, M. Swillo, and T. Wolinski, Self focusing in liquid crystalline waveguides, *Mol. Cryst. Liq. Cryst.* **320**, 157 (1998).
- [51] M. A. Karpierz, Solitary waves in liquid crystalline waveguides, *Phys. Rev. E* **66**, 036603 (2002).
- [52] M. Kwasny, U. A. Laudyn, F. A. Sala, A. Alberucci, M. A. Karpierz, and G. Assanto, Self-guided beams in low-birefringence nematic liquid crystals, *Phys. Rev. A* **86**, 013824 (2012).
- [53] N. Karimi, M. Virkki, A. Alberucci, O. Buchnev, M. Kauranen, A. Priimagi, and G. Assanto, Molding optical waveguides with nematicons, *Adv. Opt. Mater. Commun.* **5**, 1700199 (2017).
- [54] F. Simoni, *Nonlinear Optical Properties of Liquid Crystals* (World Scientific, Singapore, 1997).
- [55] I. C. Khoo, *Liquid Crystals* (John Wiley & Sons, Hoboken, 2007).
- [56] G. Giusfredi, *Physical Optics: Concepts, Optical Elements, and Techniques* (Springer Nature, Switzerland, 2019).
- [57] K. Gallo, A. Pasquazi, S. Stivala, and G. Assanto, Parametric Solitons in Two-Dimensional Lattices of Purely Nonlinear Origin, *Phys. Rev. Lett.* **100**, 053901 (2008).
- [58] G. Leo, A. Amoroso, L. Colace, G. Assanto, R. V. Roussev, and M. M. Fejer, Low-threshold spatial solitons in reverse proton exchanged PPLN waveguides, *Opt. Lett.* **29**, 1778 (2004).
- [59] W. L. Kath and N. F. Smyth, Soliton evolution and radiation loss for the Korteweg–de Vries equation, *Phys. Rev. E* **51**, 661 (1995).
- [60] A. A. Minzoni, N. F. Smyth, and A. L. Worthy, Modulation solutions for nematicon propagation in non-local liquid crystals, *J. Opt. Soc. Am. B* **24**, 1549 (2007).
- [61] D. Anderson, Variational approach to nonlinear pulse propagation in optical fibers, *Phys. Rev. A* **27**, 3135 (1983).
- [62] A. Alberucci, G. Assanto, D. Buccoliero, A. S. Desyatnikov, T. R. Marchant, and N. F. Smyth, Modulation analysis of boundary induced motion of nematicons, *Phys. Rev. A* **79**, 043816 (2009).
- [63] A. A. Minzoni, L. W. Sciberras, N. F. Smyth, and A. L. Worthy, Propagation of optical spatial solitary waves in bias-free nematic liquid crystal cells, *Phys. Rev. A* **84**, 043823 (2011).
- [64] P. Kurzynowski, W. Wozniak, and M. Szarycz, Geometric phase: Two triangles on the Poincaré sphere, *J. Opt. Soc. Am. A* **28**, 475 (2011).
- [65] I. Melendez-Montoya, D. L. Gonzalez-Hernandez, A. De Luna-Pamanes and D. Lopez-Mago, Stokes and Jones matrix polarimetry based on geometric phase measurements, *Proceedings of the SPIE, Interferometry XIX*, Vol. 10749 (SPIE, San Diego, California, 2018), pp. 400–408.
- [66] I. Melendez-Montoya, D. Gonzalez-Hernandez, A. De Luna-Pamanes, and D. Lopez-Mago, Optical polarimetry based on geometric phase measurements: unitary Jones matrix, [arXiv:1908.03829](https://arxiv.org/abs/1908.03829)
- [67] R. Schiek, Y. Baek, and G. I. Stegeman, One-dimensional spatial solitary waves due to cascaded second-order nonlinearities in planar waveguides, *Phys. Rev. E* **53**, 1138 (1996).
- [68] W. E. Torruellas, Z. Wang, D. J. Hagan, E. W. Van Stryland, G. I. Stegeman, L. Torner, and C. R. Menyuk, Observation of Two-Dimensional Spatial Solitary Waves in a Quadratic Medium, *Phys. Rev. Lett.* **74**, 5036 (1995).
- [69] G. Leo, G. Assanto, and W. E. Torruellas, Bidimensional spatial solitary waves in quadratically nonlinear bulk media, *J. Opt. Soc. Am. B* **14**, 3134 (1997).